Monthly Notices
of the
ROYAL ASTRONOMICAL SOCIETY

Mon. Not. R. Astron. Soc. **412,** 825–834 (2011) doi:10.1111/j.1365-2966.2010.17939.x

The zCOSMOS-Bright survey: the clustering of early and late galaxy morphological types since $z \simeq 1$

S. de la Torre,[1,2,3]★ O. Le Fèvre,[1] C. Porciani,[4] L. Guzzo,[2] B. Meneux,[5,6] U. Abbas,[7] L. Tasca,[3] C. M. Carollo,[8] T. Contini,[9] J.-P. Kneib,[1] S. J. Lilly,[8] V. Mainieri,[10] A. Renzini,[11] M. Scodeggio,[3] G. Zamorani,[12] S. Bardelli,[12] M. Bolzonella,[12] A. Bongiorno,[5] K. Caputi,[8] G. Coppa,[12] O. Cucciati,[1] L. de Ravel,[1] P. Franzetti,[3] B. Garilli,[3] C. Halliday,[13] A. Iovino,[2] P. Kampczyk,[8] C. Knobel,[8] A. M. Koekemoer,[14] K. Kovač,[8] F. Lamareille,[9] J.-F. Le Borgne,[9] V. Le Brun,[1] C. Maier,[8] M. Mignoli,[12] R. Pelló,[9] Y. Peng,[8] E. Perez-Montero,[9] E. Ricciardelli,[15] J. Silverman,[16] M. Tanaka,[10] L. Tresse,[1] D. Vergani,[12] E. Zucca,[12] D. Bottini,[3] A. Cappi,[12] P. Cassata,[17] A. Cimatti,[18] A. Leauthaud,[19] D. Maccagni,[3] C. Marinoni,[20] H. J. McCracken,[21] P. Memeo,[3] P. Oesch,[8] L. Pozzetti[12] and R. Scaramella[22]

[1]*Laboratoire d'Astrophysique de Marseille, 13388 Marseille, France*
[2]*INAF–Osservatorio Astronomico di Brera, 23807 Merate, Italy*
[3]*INAF–Istituto di Astrofisica Spaziale e Fisica Cosmica di Milano, 20133 Milano, Italy*
[4]*Argelander Institute for Astronomy, University of Bonn, 53121 Bonn, Germany*
[5]*Max Planck Institut für Extraterrestrische Physik, 85748 Garching, Germany*
[6]*Faculty of Physics, Universitäts-Sternwarte München, 81679 Munich, Germany*
[7]*INAF–Osservatorio Astronomico di Torino, 10025 Pino Torinese, Italy*
[8]*Institute of Astronomy, ETH Zurich, 8093 Zurich, Switzerland*
[9]*Laboratoire d'Astrophysique de l'Observatoire Midi-Pyrénées, 31400 Toulouse, France*
[10]*European Southern Observatory, 85748 Garching, Germany*
[11]*INAF–Osservatorio Astronomico di Padova, 35122 Padova, Italy*
[12]*INAF–Osservatorio Astronomico di Bologna, 40127 Bologna, Italy*
[13]*INAF–Osservatorio Astrofisico di Arcetri, 50125 Firenze, Italy*
[14]*Space Telescope Science Institute, Baltimore, MD 21218, USA*
[15]*Dipartimento di Astronomia, Universitá di Padova, 35122 Padova, Italy*
[16]*Institute for the Physics and Mathematics of the Universe, University of Tokyo, Kashiwa-shi, Chiba 277-8568, Japan*
[17]*Department of Astronomy, University of Massachusetts, Amherst, MA 01003, USA*
[18]*Dipartimento di Astronomia, Universitá di Bologna, 40127 Bologna, Italy*
[19]*Berkeley Lab & Berkeley Center for Cosmological Physics, University of California, Berkeley, CA 94720, USA*
[20]*Centre de Physique Théorique de Marseille, 13288 Marseille, France*
[21]*Institut d'Astrophysique de Paris, 75014 Paris, France*
[22]*INAF–Osservatorio Astronomico di Roma, 00040 Monte Porzio Catone, Italy*

Accepted 2010 October 28. Received 2010 October 23; in original form 2009 October 23

ABSTRACT

We measure the spatial clustering of galaxies as a function of their morphological type at $z \simeq 0.8$, for the first time in a deep redshift survey with full morphological information. This is obtained by combining high-resolution *Hubble Space Telescope* imaging and Very Large Telescope spectroscopy for about 8500 galaxies to $I_{\rm AB} = 22.5$ with accurate spectroscopic redshifts from the zCOSMOS-Bright redshift survey. At this epoch, early-type galaxies already show a significantly stronger clustering than late-type galaxies on all probed scales. A

★E-mail: sylvain.delatorre@brera.inaf.it

comparison to the Sloan Digital Sky Survey Data at $z \simeq 0.1$ shows that the relative clustering strength between early and late morphological classes tends to increase with cosmic time at small separations, while on large scales it shows no significant evolution since $z \simeq 0.8$. This suggests that most early-type galaxies had already formed in intermediate and dense environments at this epoch. Our results are consistent with a picture in which the relative clustering of different morphological types between $z \simeq 1$ and 0 reflects the evolving role of environment in the morphological transformation of galaxies, on top of a global evolution driven by mass.

Key words: galaxies: evolution – galaxies: high-redshift – galaxies: statistics – cosmology: observations – large-scale structure of Universe.

1 INTRODUCTION

In the local Universe, the clustering properties of galaxies depend on luminosity (e.g. Davis et al. 1988; Hamilton 1988; White, Tully & Davis 1988; Park et al. 1994; Loveday et al. 1995; Benoist et al. 1996; Guzzo et al. 2000; Norberg et al. 2001; Zehavi et al. 2002, 2005; Li et al. 2006; Skibba et al. 2006; Wang et al. 2007; Swanson et al. 2008), colour (e.g. Willmer, da Costa & Pellegrini 1998; Zehavi et al. 2002, 2005; Li et al. 2006; Swanson et al. 2008; Skibba & Sheth 2009), spectral type (e.g. Loveday, Tresse & Maddox 1999; Norberg et al. 2002; Madgwick et al. 2003; Wang et al. 2007) and environment (Abbas & Sheth 2006, 2007). Differences in the clustering of the various galaxy morphological types are also observed (e.g. Davis & Geller 1976; Giovanelli, Haynes & Chincarini 1986; Iovino et al. 1993; Loveday et al. 1995; Hermit et al. 1996; Guzzo et al. 1997; Willmer et al. 1998; Zehavi et al. 2002; Skibba et al. 2009). Elliptical galaxies are more strongly clustered than spiral and irregular galaxies. Another manifestation of this phenomenon is the existence of a morphology–density relation (Dressler 1980; Postman & Geller 1984), which implies that a higher fraction of ellipticals than either spirals or irregulars reside in denser environments. Spiral and irregular galaxies are more likely to populate less dense regions. However, the origin and relation between these dependences are still not fully understood. They are usually discussed in terms of a *nature* or *nurture* scenario, i.e. being intrinsic properties of galaxies at formation or originating from the interaction of galaxies with their environment all along their cosmic evolution.

At higher redshifts, our knowledge of galaxy clustering properties remains fragmentary. We know little about the clustering of the various morphological types. Deep surveys have detected an evolution in the global galaxy clustering with redshift up to $z \sim 1$–1.5 (Coil et al. 2004; Le Fèvre et al. 2005; McCracken et al. 2008). Additional results indicate that the luminosity, colour and spectral-type dependences of clustering evolve with redshift. A less significant segregation is evident when we consider the dependence of clustering on either colour or spectral type, the difference in clustering strength between red/early-type and blue/late-type galaxies being shallower at $z \sim 1$–1.5 than at $z \simeq 0$ (Meneux et al. 2006; Coil et al. 2008).

These observations are consistent with the accepted picture of hierarchical clustering growth and galaxy evolution in which CDM haloes form from the gravitational collapse of dark matter around peaks in the density field. Haloes evolve hierarchically, such that smaller haloes assemble to form larger and more massive haloes in high-density regions (Mo & White 1996; Sheth & Tormen 2002). In parallel, galaxies form within haloes, by means of the cooling of hot baryonic gas (White et al. 1987). In this framework, luminous and massive galaxies are expected to be more strongly clustered than fainter and less massive ones that tend to form in less clustered haloes, which are less biased with respect to the underlying mass distribution. Moreover, early-type galaxies, which are in general brighter than late-type galaxies, are more strongly clustered. This difference is thought to be related to their different formation histories. Early-type galaxies are understood to be the product of interaction processes (e.g. galaxy merging) and/or physical mechanisms that take place in dense environments, although mergers are more common in less dense group environments than at galaxy cluster cores (Ellison et al. 2010). However, late-type galaxies may not experience such dramatic events, being more likely to reside in less dense environments. Mergers are expected to affect galaxy morphology by creating or growing a galaxy bulge component, albeit a large gas fraction may result in a galaxy temporarily regrowing a disc. They contribute to the evolving number densities (e.g. de Ravel et al. 2009) and clustering properties of different types of galaxies.

Galaxy colours or spectral types are often used as proxies for galaxy morphologies, but are affected by uncertainties in tracing the same underlying galaxy populations across cosmic time. For instance, a disc galaxy containing an old stellar population would be classified as an early-type object. In a similar way, a starburst galaxy heavily obscured by dust would be classified as a red, early-type galaxy. In contrast, an old and red stellar population may dominate the measured stellar mass of an object, but the galaxy colour can be blue because of a recent burst of star formation. Colours are primarily related to galaxy recent star formation history at variance with morphologies, which may be the result of the interaction of galaxies with their surroundings. Selecting galaxies by colour or spectral type, or by morphology may give one different views on galaxy evolution and environmental effects at work. Studying how galaxy clustering depends on morphology and cosmic epoch may thus provide important and complementary clues to mechanisms through which galaxies developed into the population we see today. Such a study has not yet been possible at $z > 0.3$ because of the lack of high-resolution imaging surveys of sufficient size. The Cosmic Evolution Survey (COSMOS; Scoville et al. 2007) provides us with a unique sample in this respect.

In this work, we use the zCOSMOS-Bright spectroscopic sample of galaxies (Lilly et al. 2009) and measure for the first time the morphological dependence of galaxy clustering at $z \simeq 0.8$. This paper is part of a series of three papers using the first-epoch zCOSMOS-Bright sample, which investigate galaxy clustering as a function of galaxy physical properties: morphology (this paper), luminosity and stellar mass (Meneux et al. 2009) and colour (Porciani et al., in preparation).

The paper is organized as follows. In Section 2, we present the galaxy sample and its basic properties. In Section 3, we describe the method used to measure galaxy clustering. In Section 4, we provide the measurements of early- and late-type galaxy clustering.

In Section 5, we summarize and discuss our results. Throughout this paper, we assume a flat Λcold dark matter (ΛCDM) cosmology with $\Omega_{\rm M} = 0.25, \Omega_\Lambda = 0.75$ and $H_0 = 100\,h$ km s^{-1} Mpc^{-1}. The magnitudes are quoted in the AB system and for simplicity, we denote the absolute magnitude in the B band $M_B - 5\log(h)$ as M_B.

2 THE DATA

2.1 The zCOSMOS-Bright catalogue

zCOSMOS is an ongoing large spectroscopic survey being performed with the Visible Multi-Object Spectrograph (VIMOS; Le Fèvre et al. 2003) at the European Southern Observatory's Very Large Telescope (ESO-VLT). The bright part of the survey, zCOSMOS-Bright, has been designed to follow up spectroscopically the entire 1.7-deg^2 COSMOS Advanced Camera for Surveys (ACS) field (Koekemoer et al. 2007; Scoville et al. 2007) to as faint as $I_{\rm AB} = 22.5$. Observations have used the medium-resolution red grism with 1-arcsec slits, yielding a spectral resolution of $R \sim 600$ at 2.5 Å pixel^{-1}. The velocity uncertainty in the redshifts is estimated to be 110 km s^{-1}. The survey strategy, which consists of eight passes of the VIMOS spectrograph across the field, will allow us to reach in the end a high sampling rate of about 70 per cent over the entire field (Lilly et al. 2007). In the present analysis, we use the first-epoch zCOSMOS-Bright spectroscopic sample (also called *zCOSMOS 10k-bright sample*), which is based on the first 2 yr of observations performed in 2005 and 2006. The first-epoch sample covers an effective area of 1.5 deg^2 with an average sampling rate of about 30 per cent across the field. It consists of 10 644 magnitude-selected objects according to $I_{\rm AB} < 22.5$. This selection provides a redshift distribution in the range $0.1 < z < 1.2$ that peaks at $z \simeq 0.6$. A confidence class has been assigned to each object of the sample to characterize the confidence in the redshift determination and its nature. In this work, we use only galaxies with secure redshifts, i.e. objects with confidence classes 4.x, 3.x, 9.3, 9.5, 2.4, 2.5 and 1.5. Our sample thus represents 88 per cent of the full first-epoch zCOSMOS-Bright catalogue (see Lilly et al. 2009, for details). The zCOSMOS survey is able to benefit from the unprecedented multiwavelength coverage of the COSMOS field (Capak et al. 2007), which permits us to compute very accurate photometric redshifts (e.g. Ilbert et al. 2009). By incorporating the photometric redshift consistency information, we reach a spectroscopic confirmation rate of 99 per cent. The zCOSMOS survey design and the basic properties of the zCOSMOS-Bright catalogue are fully described in Lilly et al. (2007, 2009).

2.2 Galaxy morphology

A unique advantage of the COSMOS/zCOSMOS surveys is the *Hubble Space Telescope* (*HST*)-ACS high-resolution imaging (Koekemoer et al. 2007) that is available over an area of 1.7 deg^2. In particular, these data allow us to determine directly the morphology of galaxies out to $z > 1$. Morphologies used in this work were estimated using a robust classification scheme based on three non-parametric diagnostics of galaxy structure: concentration, asymmetry and the Gini coefficient (Abraham et al. 1996; Abraham, van den Bergh & Nair 2003; Lotz, Primack & Madau 2004). We first computed the distance of each galaxy in the multiparameter space with respect to each galaxy of a control sample of 500 galaxies that had been visually classified. A morphological class was then assigned to each galaxy depending on the most frequent class among those of the 11th nearest neighbours in the control sample. The choice of using this number of nearest neighbours was made as it maximizes the completeness of the different classes in our sample. Galaxies were classified into three main morphological types: early-type, spiral and irregular, with the early-type including both elliptical and lenticular galaxies (S0).

The classifier was optimized to be insensitive to band-shifting and surface brightness dimming. Since the classification is performed using a single photometric band and we study a relatively broad range of redshifts, our morphology measurements may be biased as a function of redshift because of the band-shifting effect (e.g. Lotz et al. 2004). However, as discussed in Tasca et al. (2009) our morphologies can only be affected at redshifts greater than $z \simeq 0.8$. Furthermore, the effect is small when only two broad classes of early- and late-type galaxies are defined (Brinchmann et al. 1998), which is the case here. In practice, spiral galaxies can be misclassified as irregulars but, since we define a broad class of late-type galaxies that includes both spiral and irregular galaxies, our analysis is unaffected by this bias. We evaluated the contamination and completeness of the different classes by applying our automated classifier to the control sample and comparing the resulting classification with the visual one. This comparison showed that our classification scheme is rather robust with only a small contamination of about 7 per cent for each class when considering only two broad classes of early-type and spiral+irregular galaxies. We verified, using more conservative morphological classes with almost no contamination but larger incompleteness (i.e. the 'clean' sample of Tasca et al. 2009), that this has a limited impact on the clustering measurements. The effect is much smaller than the statistical error on $w_{\rm p}(r_{\rm p})$ measurements. We refer the reader to Tasca et al. (2009) for a full description of the classification scheme and the properties of the morphological sample.

In this study, we focus on two broad classes: early types and late types, the latter referring to galaxies morphologically classified as either spirals or irregulars. Because of the slightly different geometries of the COSMOS-ACS and zCOSMOS-Bright fields, a small number of galaxies in the zCOSMOS-Bright catalogue do not have morphological measurements. These galaxies, which represent 3 per cent of the zCOSMOS-Bright sample, are indicated by crosses in Fig. 1. In this analysis, we therefore remove galaxies that do not have a counterpart in the COSMOS-ACS photometric catalogue (Leauthaud et al. 2007). In the end, the effective area of the sample that we can use is defined to be the intersection of the COSMOS-ACS and zCOSMOS fields, after removal of regions affected by photometric defects for which no morphological measurement is available (see Fig. 1).

2.3 Sample selection

We consider a nearly volume-limited sample where galaxies are selected to be of absolute magnitude below a given threshold and to populate a complete comoving volume in the considered redshift interval. We focus on the high-redshift part of the zCOSMOS-Bright sample, defining volume-limited samples of early- and late-type galaxies at $0.6 < z < 1.0$. The selection is performed on the basis of the galaxy B-band absolute magnitudes to facilitate comparison with other studies. We include an intrinsic luminosity evolution in the definition of the sample by considering a linearly evolving absolute magnitude cut such as

$$M_B < -20.4 - Q(1.0 - z), \quad (1)$$

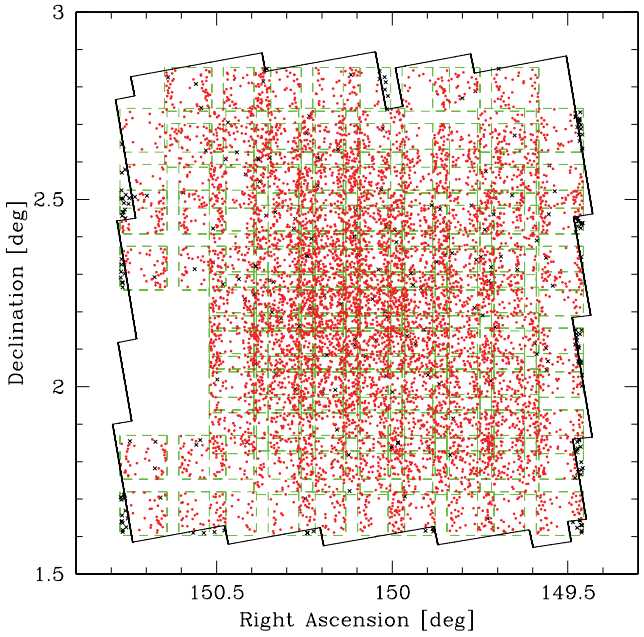

Figure 1. Angular distribution of the zCOSMOS-Bright sample. The solid line shows the boundary of the COSMOS-ACS survey and the dashed contours encompass the regions observed by VIMOS during the zCOSMOS-Bright first-epoch observations. Crosses indicate the few galaxies for which no morphological information is available because they either lie outside the COSMOS-ACS field or coincide with photometric defects in the images.

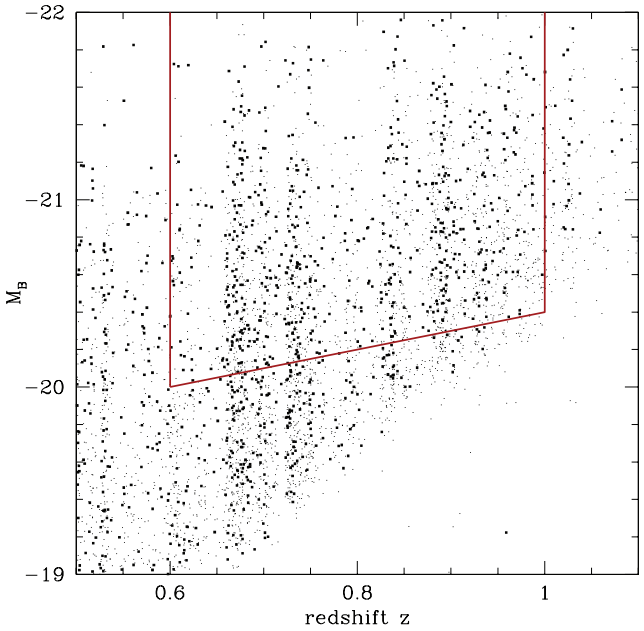

Figure 2. Distribution of the zCOSMOS-Bright galaxies in the *B*-band absolute magnitude–redshift plane. Early-type galaxies are indicated by squares and late-type galaxies by dots. The solid line shows the boundary of the defined volume-limited sample.

where Q is a constant, as shown in Fig. 2. This is performed to ensure that the evolution in the characteristic galaxy luminosity within the considered redshift interval is taken into account. This absolute magnitude threshold allows us to select galaxies with luminosities above L^* at these redshifts. The mean luminosity of all galaxies selected above this threshold is about $1.1L^*$ (Zucca et al. 2009).

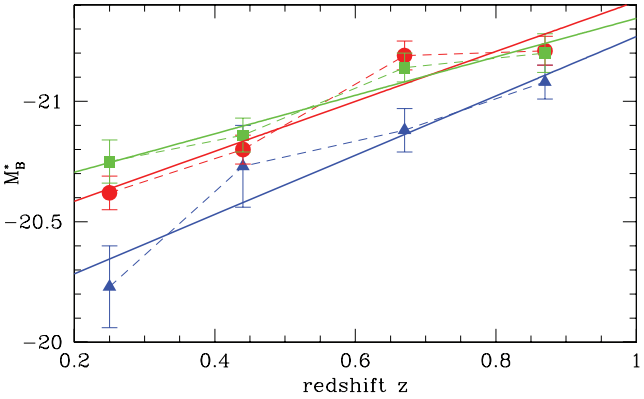

Figure 3. Evolution of the characteristic absolute magnitude in the *B* band, M_B^*, as a function of redshift as measured by Zucca et al. (2009) for early-type (circles), spiral (squares) and irregular (triangles) galaxies in the zCOSMOS-Bright sample. The lines correspond to the best-fitting linear evolution of $M_B^*(z)$ for the three morphological types.

Different galaxy populations exhibit different luminosity evolutions (Lilly et al. 1996; Zucca et al. 2006) and thus Q depends on the morphological type. The value of Q can be inferred observationally from the evolution of the luminosity function for the different morphological types. We used the characteristic absolute magnitude in the *B* band, M_B^*, derived from the same data by Zucca et al. (2009) in different redshift intervals and for different morphological types. We note that we used M^* values obtained by keeping the faint-end slope of the luminosity function α fixed. This is a reasonable decision since α does not clearly exhibit any type of evolution at these redshifts (Zucca et al. 2009). We adopted this approach to avoid compensating for the luminosity evolution with an artificial increase in α.

We therefore determined Q by fitting the redshift evolution in M_B^* with a linear function. The values of $M_B^*(z)$ for the three morphological types and their best-fitting linear functions are presented in Fig. 3. We find a small amount of luminosity evolution for early types and spirals, given, respectively, by $Q_E = -1.04 \pm 0.22$ and $Q_S = -0.80 \pm 0.14$, but a stronger evolution for irregular galaxies, for which $Q_I = -1.23 \pm 0.24$. In the case of irregular galaxies, the value of Q is driven significantly in the fit by the low-redshift point, which has a relatively small and unexpected value. Excluding this point in the fit yields a higher value of $Q_I = -0.84 \pm 0.11$, close to that found for spirals. Therefore, after several tests and given the large uncertainty in these values, we assumed that $Q = -1$ for all morphological types, which is close to the average of the three morphological classes. We directly tested that varying the slope of the absolute magnitude cut removes or adds only a small fraction of galaxies and does not influence significantly the measurements of the correlation function.

3 GALAXY CLUSTERING ESTIMATION

3.1 The projected two-point correlation function

To estimate galaxy clustering, we use the standard projected two-point projected correlation function $w_p(r_p)$, which enables us to measure real-space clustering without being affected by redshift-space distortions. The three-dimensional galaxy distribution that is recovered from redshift surveys and its two-point correlation function $\xi(s)$ are distorted because of the effect of galaxy peculiar motions. These motions affect in particular the distance

measurements in the radial direction. By dividing the vector $\boldsymbol{s}$ into two components, $\boldsymbol{r}_\mathrm{p}$ and $\boldsymbol{\pi}$, respectively, perpendicular and parallel to the line of sight (Peebles 1980; Fisher et al. 1994), one obtains the bidimensional two-point correlation function $\xi(r_\mathrm{p}, \pi)$. One can then recover the true spatial correlations by integrating over the redshift-space distortion field, projecting $\xi(r_\mathrm{p}, \pi)$ along the line of sight. The projected two-point correlation function $w_\mathrm{p}(r_\mathrm{p})$ is related to both $\xi(r_\mathrm{p}, \pi)$ and the real-space two-point correlation function $\xi(r)$ by the relations

$$w_\mathrm{p}(r_\mathrm{p}) = 2\int_0^\infty \xi(r_\mathrm{p}, \pi)\mathrm{d}\pi = 2\int_{r_\mathrm{p}}^\infty \frac{\xi(r)}{\left(r^2 - r_\mathrm{p}^2\right)^{1/2}} r\mathrm{d}r. \quad (2)$$

To compute $w_\mathrm{p}(r_\mathrm{p})$, we chose in practice to integrate $\xi(r_\mathrm{p}, \pi)$ out to $\pi_\mathrm{max} = 20\,h^{-1}$ Mpc. Given the volume of the survey, we found that this value is sufficiently large and optimally minimizes the noise introduced at large π by the uncorrelated pairs in the data (see also Meneux et al. 2009; Porciani et al., in preparation). This truncation introduces a global underestimation of $w_\mathrm{p}(r_\mathrm{p})$ of about 10 per cent that has to be taken into account when modelling the observations.

We computed $\xi(r_\mathrm{p}, \pi)$ using the standard Landy & Szalay (1993) estimator, which is defined by

$$\xi(r_\mathrm{p}, \pi) = \frac{GG(r_\mathrm{p}, \pi) - 2GR(r_\mathrm{p}, \pi) + RR(r_\mathrm{p}, \pi)}{RR(r_\mathrm{p}, \pi)}, \quad (3)$$

where $GG(r_\mathrm{p}, \pi)$, $RR(r_\mathrm{p}, \pi)$ and $GR(r_\mathrm{p}, \pi)$ are, respectively, the normalized numbers of distinct galaxy–galaxy, galaxy–random and random–random pairs with comoving separations between $[r, r + \mathrm{d}r]$ and $[\pi, \pi + \mathrm{d}\pi]$. In this analysis, we used random samples of 90 000 objects.

3.2 Observational biases

The zCOSMOS-Bright sample has a complex angular sampling because of the survey observational strategy and the shape of the VIMOS field of view. In Fig. 1, one can discern the VIMOS footprint and the superposition of multiple passes in the angular distribution of galaxies. To correct the projected correlation function for this non-uniform and incomplete angular sampling, we accurately estimated the background counts expected for unclustered objects in the field. We generated random catalogues with the detailed angular selection function of the sample by varying the number of random galaxies with angular position. More precisely, from the knowledge of the precise shape of the VIMOS field of view and the coordinates of the observed pointings, we distribute iteratively random galaxies inside the areas covered by each pointing. With this procedure, we reproduce in the random sample the effective surface density variations due to the non-uniform spectroscopic sampling of the zCOSMOS sample, illustrated in Fig. 4. The objects within regions of the parent photometric catalogue affected by photometric defects, and for which no morphological measurements were possible, were removed a posteriori by applying the COSMOS-ACS photometric mask (Leauthaud et al. 2007). This technique was already applied to the clustering analysis of the VIMOS-VLT Deep Survey (VVDS; e.g. Le Fèvre et al. 2005; Meneux et al. 2006; Pollo et al. 2006; de la Torre et al. 2007), which suffers from similar observational biases (see Pollo et al. 2005, for details). In the present analysis, we improve this method by adding a correction for the non-uniform sampling inside each pointing and including a more accurate pair-weighting scheme to correct for the angular incompleteness, as described below.

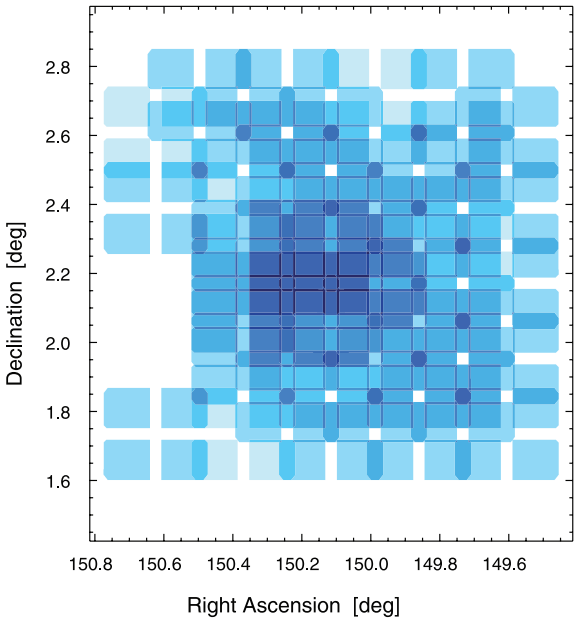

Figure 4. Variation in the angular sampling of the zCOSMOS-Bright sample. The colour darkness encodes the number of passes of the VIMOS spectrograph on the sky during zCOSMOS-Bright first-epoch observations. The dark colour at the centre of field corresponds to the VIMOS eight-passes coverage expected over the full area in the final zCOSMOS-Bright sample.

In the top panel of Fig. 5, we plot the distribution of zCOSMOS-Bright galaxies in the rest-frame angular coordinates of their pointing. The solid contours correspond to the effective shape of the four quadrants of the VIMOS field of view. In this figure, one can discern a variation in sampling as a function of the position within the pointing, in the right ascension direction. This non-uniform sampling is produced during the designing of slit masks to optimize the total number of slits, and in turn produces two layers of spectra in each mask (Bottini et al. 2005). This problem is more severe for zCOSMOS-Bright than VVDS because of the use of a higher resolution grism and consequently longer spectra on the detector, which limit the degree of freedom of the slit positioning algorithm. We therefore correct for this by reproducing within the random samples the right-ascension-dependent sampling of each pointing. We model the average distribution of galaxies along the right ascension direction with a smooth function, as shown in the bottom panel of Fig. 5, and use the fitted model to distribute the galaxies in the random sample.

In addition, we use a pair-weighting scheme to account for the small-scale incompleteness caused by the geometrical constraints of the slit mask design (Bottini et al. 2005), which prevent VIMOS from simultaneously targeting very close objects. As shown in the top panel of Fig. 6, in general this incompleteness affects the angular clustering on scales of $\theta < 0.^\circ02$, but the effect becomes significant only below $\theta = 0.^\circ004$. The latter angular scale corresponds to a maximum separation of $r_\mathrm{p} = 0.17\,h^{-1}$ Mpc at $0.6 < z < 1.0$. To correct for this, we assign a weight to each galaxy–galaxy pair that accounts for the missed angular pairs. To calculate the weights, we use the information contained in the parent photometric catalogue, which is assumed to be free from angular incompleteness. We define a weighting function $f(\theta)$ to be the ratio of the mean number of pairs in the parent photometric catalogue to those in the spectroscopic catalogue as a function of angular separation. This quantity can be

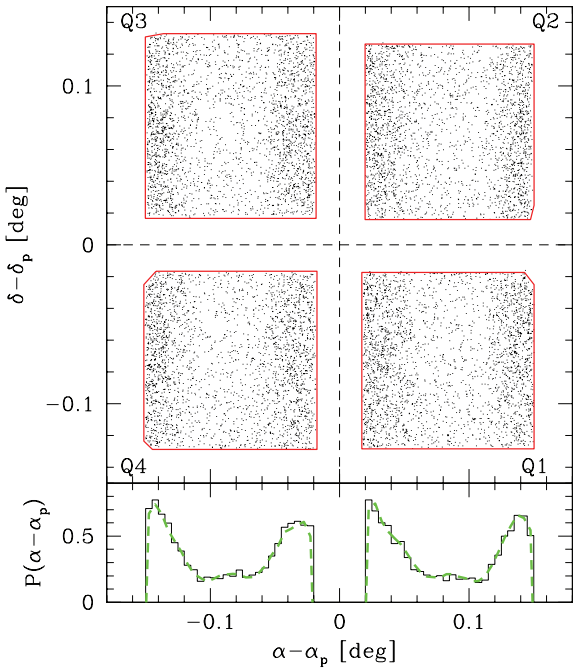

Figure 5. Top panel: distribution of the zCOSMOS-Bright galaxies in the rest-frame angular coordinates of their pointing, showing the uneven coverage of each of the four VIMOS quadrants. Bottom panel: corresponding histogram along the right ascension direction. The dashed curve is the smooth function used to model the average galaxy distribution along the right ascension direction within each pointing.

written as (e.g. Hawkins et al. 2003),

$$f(\theta) = \frac{1 + w_{\rm par}(\theta)}{1 + w_{\rm spec}(\theta)}, \tag{4}$$

where $w_{\rm par}(\theta)$ and $w_{\rm spec}(\theta)$ are the angular correlation functions of the parent photometric and spectroscopic samples, respectively. We again use the Landy & Szalay (1993) estimator to compute the angular correlation functions. In the calculation of $w_{\rm spec}(\theta)$, we account for the complex angular sampling of the spectroscopic catalogue, as discussed above. We note that only the galaxy–galaxy pairs are weighted because the random sample does not have any close-pair constraints. The weighting function and the angular correlation functions of the parent photometric and spectroscopic samples are shown in Fig. 6. We compared this weighting scheme with those adopted in the parallel clustering analyses by Meneux et al. (2009) and Porciani et al. (in preparation) and found that the different estimators yield consistent results within the errors. More detailed results of this comparison are presented in Porciani et al. (in preparation).

Finally, to compute $\xi(r_{\rm p}, \pi)$, the random catalogues also need to reproduce the detailed radial selection function of the survey. Galaxies are clustered and, because the volumes probed by galaxy surveys are usually small, it is difficult to measure average quantities such as the radial distribution of objects. The subsequent variability in the measurements, usually referred to as sample variance (or cosmic variance), can significantly bias its determination (e.g. Garilli et al. 2008). One way of obtaining the radial selection function entails convolving the observed galaxy redshift distribution with a kernel of sufficiently large width to smooth out the resolved structures. The zCOSMOS-Bright sample contains a large number of structures along the line of sight that correspond to the multiple peaks seen in the observed radial distribution. We find that the smoothing method tends to flatten and broaden the redshift distribution in our sample. A Gaussian filter of smoothing length as large as $\sigma_{\rm s} = 450\,h^{-1}$ Mpc needs to be applied to completely remove the spikes in the radial distribution. This, however, distorts the shape of the radial distribution as shown in Fig. 7. An alternative way of estimating the expected $N(z)$ that we adopt here is to use the galaxy luminosity function. For volume-limited samples, one can recover the radial distribution $N(z)$ as

$$N(z){\rm d}z = \int_{-\infty}^{M_{\rm max}} \phi(M, z)\frac{{\rm d}V_{\rm c}}{{\rm d}z}{\rm d}M{\rm d}z, \tag{5}$$

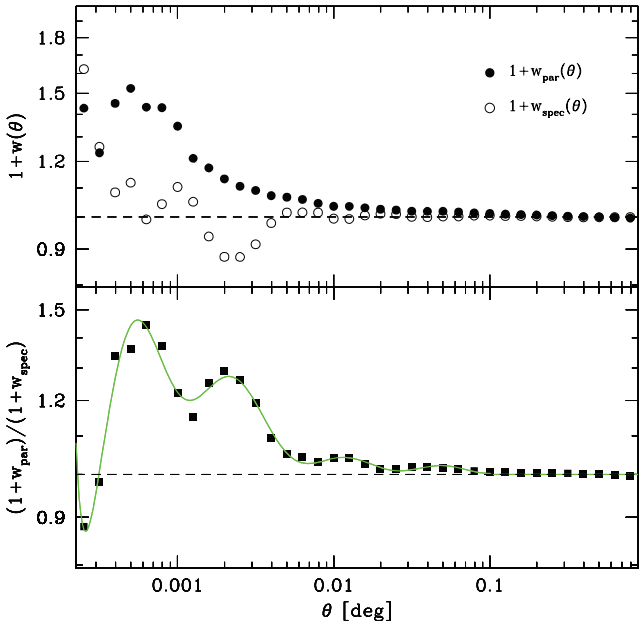

Figure 6. Top panel: angular correlation functions of the parent photometric catalogue $w_{\rm p}(\theta)$ (solid points) and the spectroscopic catalogue $w_{\rm s}(\theta)$ (open points). Bottom panel: ratio of these two functions, where the weighting function (solid curve) was used to correct for the angular incompleteness.

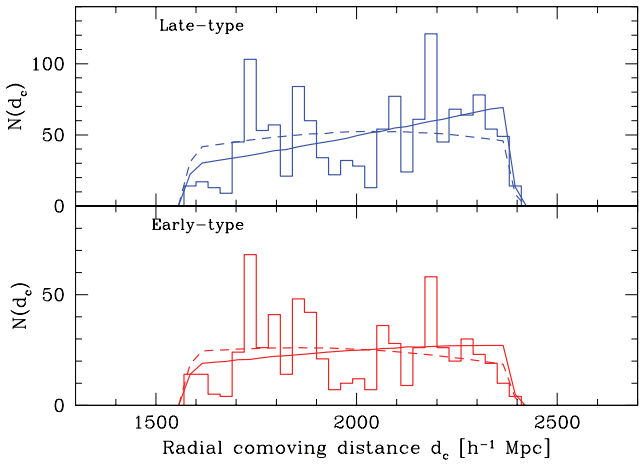

Figure 7. Observed radial distribution in our volume-limited sample at $0.6 < z < 1.0$ (histogram) for late-type (top panel) and early-type (bottom panel) galaxies. The dashed curve shows the distribution obtained by smoothing the observed radial distribution with a Gaussian filter using a smoothing length of $\sigma_{\rm s} = 450\,h^{-1}$ Mpc. The solid curve corresponds to the distribution derived by integrating the galaxy luminosity function.

where $\phi(M, z)$ is the galaxy luminosity function at redshift z and V_c is the comoving volume. In practice, to obtain $\phi(M, z)$, we first fitted the evolution of the measured Schechter parameters in different redshift bins by Zucca et al. (2009) with linear functions of z. We then use the functions that best describe $\phi^*(z)$, $M^*(z)$ and $\alpha(z)$ to obtain $\phi(M, z)$ at any redshift z, assuming a Schechter form of the luminosity function. This method has the advantage of reducing sample variance effects in the determination of the radial distribution by smoothing out the spurious variations in the measured Schechter parameters from one redshift bin to another. The resulting predicted radial distribution using this method is also shown in Fig. 7.

3.3 Error estimation

We estimate the errors in the correlation function measurements using the blockwise bootstrap method (e.g. Porciani & Giavalisco 2002), which provides a reliable estimate of both the statistical and sample variance errors. We verified their reliability by directly comparing with the ensemble average scatter of a set of mock samples of the survey and chose blockwise errors because they produced a more stable covariance matrix. This internal-error estimator consists in calculating the variance in the correlation functions among a given number of realizations $N_{\rm real}$ of the sample, consisting of a random sequence of $N_{\rm sub}$ equal-sized sub-volumes, allowing for repetitions. To define the sub-volumes and because the transverse dimension of the survey is small, we divided the sample into slices along the radial direction and constrained the radial size of each slice to be larger than five times $\pi_{\rm max}$, as defined in Section 3.1. Therefore, for each sample, we generated $N_{\rm real} = 800$ realizations by bootstrapping $N_{\rm sub} = 8$ slices of equal volume.

Norberg et al. (2009) studied the efficiency of different error estimators, showing that this particular technique enables us to robustly recover the main eigenvectors of the underlying covariance matrix and that by obtaining a large number of realizations $N_{\rm real} > 3N_{\rm sub}$, one can calculate variances that agree with external estimators. However, their analysis is performed by considering significantly larger volumes than the one probed by the zCOSMOS-Bright sample, which prompted us to check directly the reliability of this method for our specific survey using mock samples. We used 24 realistic mock samples of the COSMOS survey provided by Kitzbichler & White (2007) and based on the Millennium dark matter N-body simulation (Springel et al. 2005). We applied to them the detailed zCOSMOS-Bright observational strategy. For this purpose, we used SSPOC software (Bottini et al. 2005) to mimic in the mock samples the selection of spectroscopic targets within the observed pointings. In addition, we included the same redshift success rate as the real data (see Iovino et al. 2010, for details). We find that the blockwise bootstrap method, on average, allows us to recover fairly well both the diagonal and off-diagonal terms of the covariance matrix, although the diagonal errors are slightly underestimated on large scales. This effect is, however, of the order of 20–25 per cent on scales between 2 and $10\,h^{-1}$ Mpc. Details of the error analysis are presented in Meneux et al. (2009) and Porciani et al. (in preparation).

4 RESULTS

We present in Fig. 8 our measurement of the spatial clustering of early- and late-type galaxies at $\bar{z} = 0.81$, showing that at this epoch the former are already more strongly clustered than the latter. The observed segregation tends to only affect the amplitude of the projected correlation function on all probed scales, corresponding to an almost scale-independent relative clustering of early- to late-type galaxies that we discuss in Section 4.2. We compare our measurements with those obtained by Skibba et al. (2009) at $z \simeq 0.1$ in the Sloan Digital Sky Survey (SDSS) Data Release 6 (Adelman-McCarthy et al. 2008) and based on visually classified morphologies from the Galaxy Zoo sample (Lintott et al. 2008). We overplot in Fig. 8 the $w_{\rm p}(r_{\rm p})$ measurements they obtained for early and late morphological types (defined as $P_{\rm el} > 0.8$ and $P_{\rm sp} > 0.8$, respectively; see Skibba et al. 2009), with absolute magnitudes of $M_r < -20.5$. This magnitude cut selects galaxies with luminosity above L^* at $z \simeq 0.1$ (Blanton et al. 2003), making these local measurements comparable with ours. However, we cannot make a fully quantitative comparison as the sample selection and morphological classifications are not exactly the same. Comparison of the correlation function shapes shows some indications of an increase with cosmic time in the relative difference in clustering between early and late morphological classes for separations smaller than a few h^{-1} Mpc, although error bars are relatively large on these scales in our sample.

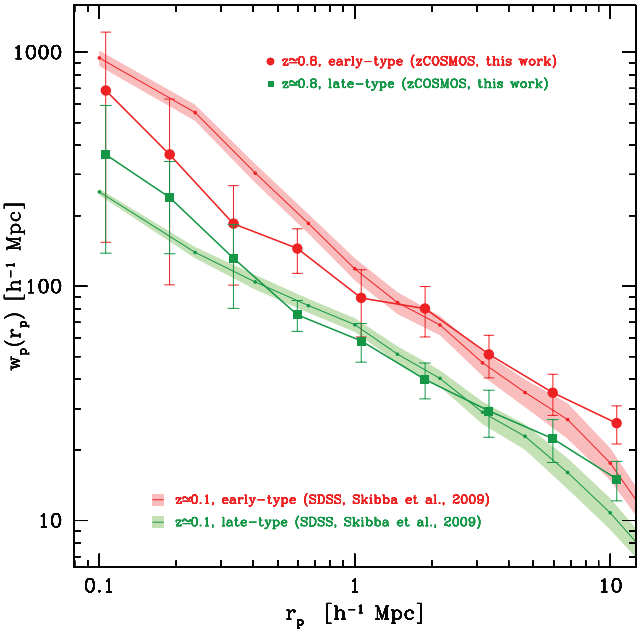

Figure 8. The projected correlation functions of early types (circles) and late types (squares) in our volume-limited sample at $0.6 < z < 1.0$. The solid lines correspond to the measurements of Skibba et al. (2009) at $z \simeq 0.1$.

4.1 Effect of the overabundance of high-density regions in the COSMOS field

In the measurements of Fig. 8, the shape of the projected correlation function at $r_{\rm p} > 1\,h^{-1}$ Mpc, for both early- and late-type galaxies, is flatter than that for the SDSS, with approximately $w_{\rm p}(r_{\rm p}) \propto r_{\rm p}^{-1.6}$. Such behaviour was also noticed in previous analysis of the zCOSMOS-Bright data, based on luminosity- and stellar-mass-selected samples (Meneux et al. 2009), and has been recently explained as being due to an overabundance of rich structures in the field, in particular at $z > 0.6$ (de la Torre et al. 2010). This is quantified by an excess of galaxies in the high-density tail of the overdensity probability distribution function of the sample, which is responsible for an enhancement of the clustering signal on scales above 1–2 h^{-1} Mpc. de la Torre et al. (2010) found that simply

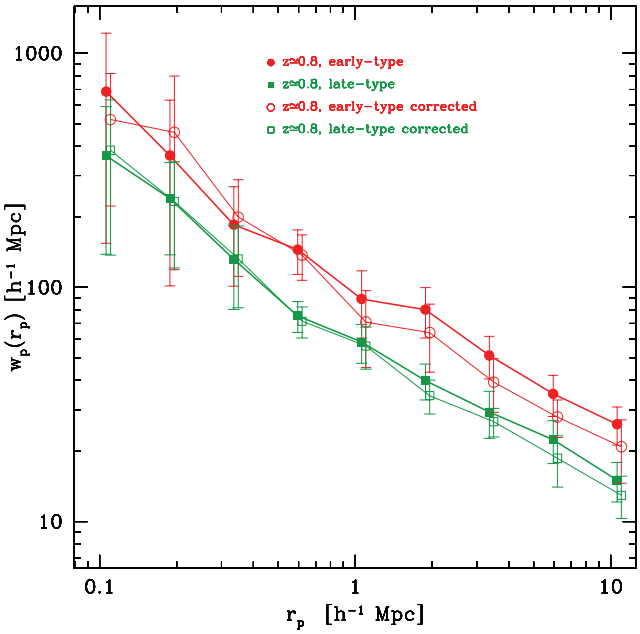

Figure 9. The projected correlation functions of early types (circles) and late types (squares) in our volume-limited sample at $0.6 < z < 1.0$. The empty circles (for early types) and empty squares (for late types) are obtained while removing all the galaxies inhabiting the rich structures in excess in the zCOSMOS sample (see the text for details). The latter points have been slightly displaced along the r_p-axis to improve the clarity of the figure.

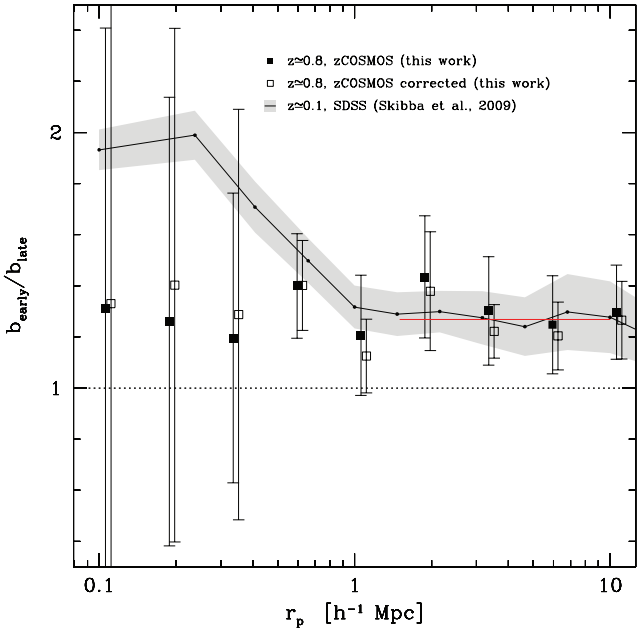

Figure 10. Relative clustering of early- to late-type galaxies as a function of scale in our sample (symbols), compared to that at $z \simeq 0.1$ obtained from Skibba et al. (2009) measurements (solid curve). The amplitude of the solid line defines the large-scale linear relative bias of early- to late-type galaxies, i.e. the plateau measured in the range $1.5\,h^{-1}$ Mpc $< r_p < 10\,h^{-1}$ Mpc. The empty squares show the relative bias obtained while removing all the galaxies inhabiting the rich structures in excess in the zCOSMOS sample (see the text for details).

removing galaxies inhabiting the 10 per cent densest environments brings the shape of $w_p(r_p)$ back into agreement with current ΛCDM model predictions and other data sets (Meneux et al. 2008, 2009). We explore the significance of this effect in our morphologically selected samples performing exactly the same operation here. The resulting $w_p(r_p)$ are shown as empty symbols in Fig. 9. This procedure reduces the amplitude of $w_p(r_p)$ on large scales, although the result is less dramatic than in the full sample (de la Torre et al. 2010), and allows us to obtain better-behaved $w_p(r_p)$ shapes on these scales.

4.2 Relative clustering of early- to late-type galaxies

The observed relative clustering between different galaxy types can provide us with valuable information on the properties of the galaxy formation bias (e.g. Narayanan Berlind & Weinberg 2000). In general, local biasing models predict constant scale-independent relative clustering on large scales (Coles 1993; Fry & Gaztanaga 1993; Mann et al. 1998; Scherrer & Weinberg 1998; Narayanan et al. 2000). This prediction remains in any model where the galaxy type is correlated with the local density. We note that here 'local' refers to scales over which material in non-linear structures has mixed during the cosmic history. This behaviour disagrees with models of non-local bias in which, for instance, the galaxy formation efficiency is coherently modulated over large scales because of ionizing radiation (Bower et al. 1993) or suppressed in randomly distributed voids (Babul & White 1991). In these models, the large-scale relative clustering is expected to be scale-dependent (Narayanan et al. 2000).

Fig. 10 shows the relative clustering (or relative bias) $b_{rel}(r_p)$ of early- to late-type galaxies in the range $0.1\,h^{-1}$ Mpc $< r_p < 10\,h^{-1}$ Mpc obtained in our sample and from SDSS measurements as

$$b_{rel} = \left(\frac{w_p^{early}}{w_p^{late}}\right)^{\frac{1}{2}} = \left(\frac{w_p^{early}}{w_p^{m}}\frac{w_p^{m}}{w_p^{late}}\right)^{\frac{1}{2}} = \frac{b_{early}}{b_{late}}, \quad (6)$$

where w_p^{early} and b_{early} (w_p^{late} and b_{late}) correspond, respectively, to the projected correlation function and the bias of early-type (late-type) galaxies with respect to the mass and w_p^{m} is the projected correlation function of mass. At $z \simeq 0.1$, the relative bias shows a scale dependence in the regime where clustering is non-linear, i.e. on small scales, but tends asymptotically to a constant value on larger scales. It varies from $b_{rel} \simeq 2$ at $r_p \simeq 0.2\,h^{-1}$ Mpc to $b_{rel} \simeq 1.3$ at $r_p \simeq 5\,h^{-1}$ Mpc, confirming previously reported clustering measurements in the local Universe (Loveday et al. 1995; Hermit et al. 1996; Guzzo et al. 1997; Willmer et al. 1998). The observed large-scale behaviour of the relative bias then supports a locally biased galaxy formation scenario, in which the definition of early and late morphological types may be directly or indirectly related to the local environment. Moreover the large value of the relative bias on small scales, i.e. below $1\ h^{-1}$ Mpc, suggests that a fraction of early-type galaxies formed recently and preferentially in dense environments. At $z \simeq 0.8$, in contrast, the scale dependence is much less important or absent. These results may indicate that a fraction of early-type galaxies may have formed at epochs later than $z \simeq 0.8$ by the merging of late-type galaxies (perhaps through major mergers), in relatively dense environments.

From the relative bias of early- to late-type galaxies, we derived the large-scale linear relative bias b_{rel}^{lin} by averaging $b_{rel}(r_p)$ on scales of $1.5\,h^{-1}$ Mpc $< r_p < 10\,h^{-1}$ Mpc. Our measurement, corrected for the effect of the excess of rich structures in the field, is reported in Table 1 where it is compared with $z \simeq 0$ measurements. Interestingly, we find in our sample a value of b_{rel}^{lin} similar to that measured in the

Table 1. Large-scale relative bias of early- to late-type galaxies. These values are obtained by averaging the relative bias of early- to late-type galaxies between 1.5 and $10\,h^{-1}$ Mpc.

$\bar{z}$	Selection	$\bar{L}/L^*$	$b_{\rm rel}^{\rm lin}$	Reference
0.8	$M_B < -20.4 + (1.0 - z)$	1.1	1.27 ± 0.16	This work
0.1	$M_r < -20.5$	1.1	1.26 ± 0.12	(1) Skibba et al. (2009)
$\sim$0	$M_B < -19.5$	1	1.19 ± 0.25	(2) Willmer et al. (1998)
$\sim$0	$M_B < -19.5$	1	1.53 ± 0.19	(3) Guzzo et al. (1997)
$\sim$0	$M_j \simeq -19.5$	0.9	1.26 ± 0.36	(4) Loveday et al. (1995)

Note. For references (2), (3) and (4), the large-scale relative bias is calculated from the power-law best fits to the $w_{\rm p}(r_{\rm p})$ of elliptical/S0 (early-type) and spiral (late-type) galaxies; errors are obtained by propagating errors in the individual power-law parameters.

local samples and in particular in the SDSS. This finding suggests that most of the dependence of galaxy clustering on morphology was already in place at $z \simeq 0.8$ for $L > L^*$ galaxies.

5 SUMMARY AND DISCUSSION

We have measured the dependence of clustering on morphology at $0.6 < z < 1.0$ for galaxies of luminosity greater than L^*. For this purpose, we have used the first-epoch zCOSMOS-Bright spectroscopic sample of galaxies, our study benefiting from the availability of high-resolution *HST* imaging for the COSMOS field. We have computed the projected correlations' function in volume-limited samples of two broad morphological classes, early types (elliptical/S0) and late types (spiral/irregular), and have compared them to $z \simeq 0.1$ SDSS measurements. Our two main results can be summarized as follows.

(i) We find that at $z \simeq 0.8$, early-type galaxies exhibit stronger clustering strength than late-type galaxies on scales from 0.1 to $10\,h^{-1}$ Mpc.

(ii) Comparing our results to those for the SDSS for galaxies with comparable luminosities shows that while the relative difference in clustering between early and late morphological classes seems to increase with cosmic time on scales smaller than a few h^{-1} Mpc, the large-scale difference does not evolve significantly since $z \simeq 0.8$. This indicates that a large fraction of early-type galaxies were already formed in intermediate and dense environments at this epoch.

The observed difference in the shape of the correlation function that we observe for early- and late-type galaxies can be interpreted within the framework of halo occupation distribution models (e.g. Cooray & Sheth 2002). In these models, the galaxy correlation function is the sum of two contributions, a small-scale contribution, which characterizes the clustering of galaxies inside haloes (one-halo term), and a large-scale contribution, which characterizes the clustering of galaxies belonging to different haloes (two-halo term). The prominence of the one-halo term observed for early-type galaxies, i.e. the enhancement of the observed correlation function on scales smaller than or of the order of the typical halo radius (1–$2\,h^{-1}$ Mpc), implies that these galaxies are on average hosted by massive haloes with larger virial radii in dense environments (Abbas & Sheth 2006). The weaker but steeper one-halo term of late-type galaxies indicates that these galaxies may instead be hosted on average by less massive haloes inhabiting low-density environments. This trend is qualitatively consistent with $z \simeq 0$ measurements of the clustering of red and blue galaxies, which dominate respectively the early- and late-type populations (e.g. Zehavi et al. 2005; Skibba & Sheth 2009).

Our work is complementary to those of Tasca et al. (2009) and Kovač et al. (2010) who study within the same sample the evolution of the fraction of early and late morphological types with environment, as defined by either the continuous overdensity field or group/field environments, respectively. The measurements presented here are consistent with the picture emerging from these works. In particular, Tasca et al. (2009) observed a flattening in the morphology–density relation with increasing redshift at fixed luminosity, a similar trend to that observed in the colour–density and spectral-type–density relations (Cooper et al. 2006; Cucciati et al. 2006; Grützbauch et al. 2010). The finding that early- and late-type galaxies tend to have increasingly similar probabilities of populating high-density/group and low-density/field environments with increasing redshift is qualitatively consistent with the evolution in the morphological dependence of clustering discussed here, where we find a corresponding decrease in the relatively small-scale clustering of early- to late-type galaxies. The mass and environmental physical processes play an important role in shaping the morphology–density relation and its evolution with cosmic time (e.g. Kovač et al. 2010). It is found that mass has a dominant contribution at $z \simeq 1$, in particular for a relatively bright luminosity-selected sample (Tasca et al. 2009). In contrast, in the local Universe, one finds that only a part of this relation can be attributed to the variation in the stellar-mass function with environment, with the dense environment-related processes becoming more important (Bamford et al. 2009). Our results corroborate this evolutionary picture. While the large-scale shape of the relative bias has remained almost constant since $z \simeq 1$, the small-scale shape exhibits a significant evolution. This is due to an increase in the number of small-scale early-type pairs with cosmic time, as a result of the relative contribution of environmental physical processes in transforming early- to late-type galaxies, especially in dense environments.

ACKNOWLEDGMENTS

We acknowledge the anonymous referee for his careful review of the paper and helpful suggestions. Financial support from INAF and ASI through grants PRIN-INAF-2007 and ASI/COFIS/WP3110 I/026/07/0 is gratefully acknowledged. JS is supported by World Premier International Research Center Initiative (WPI Initiative), MEXT, Japan.

This work is based on observations undertaken at the ESO-VLT under Large Program 175.A-0839 and also on observations with the NASA/ESA *HST*, obtained at the Space Telescope Science Institute, operated by the Association of Universities for Research in Astronomy, Inc. (AURA), under NASA contract NAS 5Y26555, with the Subaru Telescope, operated by the National Astronomical Observatory of Japan, with the telescopes of the National Optical Astronomy Observatory, operated by the Association of Universi-

ties for Research in Astronomy, Inc. (AURA), under cooperative agreement with the National Science Foundation, and with the Canada–France–Hawaii Telescope, operated by the National Research Council of Canada, the Centre National de la Recherche Scientifique de France and the University of Hawaii.

REFERENCES

Abbas U., Sheth R. K., 2006, MNRAS, 372, 1749
Abbas U., Sheth R. K., 2007, MNRAS, 378, 641
Abraham R. G., van den Bergh S., Glazebrook K., Ellis R. S., Santiago B. X., Surma P., Griffiths R. E., 1996, ApJS, 107, 1
Abraham R. G., van den Bergh S., Nair P., 2003, ApJ, 588, 218
Adelman-McCarthy J. K. et al., 2008, ApJS, 175, 297
Babul A., White S. D. M., 1991, MNRAS, 253, 31P
Bamford S. P. et al., 2009, MNRAS, 393, 1324
Benoist C., Maurogordato S., da Costa L. N., Cappi A., Schaeffer R., 1996, ApJ, 472, 452
Blanton M. R. et al., 2003, ApJ, 592, 819
Bottini D. et al., 2005, PASP, 117, 996
Bower R. G., Coles P., Frenk C. S., White S. D. M., 1993, ApJ, 405, 403
Brinchmann J. et al., 1998, ApJ, 499, 112
Capak P. et al., 2007, ApJS, 172, 99
Coil A. L. et al., 2004, ApJ, 609, 525
Coil A. L. et al., 2008, ApJ, 672, 153
Coles P., 1993, MNRAS, 262, 1065
Cooper M. C. et al., 2006, MNRAS, 370, 198
Cooray A., Sheth R., 2002, Phys. Rep., 372, 1
Cucciati O. et al., 2006, A&A, 458, 39
Davis M., Geller M. J., 1976, ApJ, 208, 13
Davis M., Meiksin A., Strauss M. A., da Costa L. N., Yahil A., 1988, ApJ, 333, L9
de la Torre S. et al., 2007, A&A, 475, 443
de la Torre S. et al., 2010, MNRAS, 409, 867
de Ravel L. et al., 2009, A&A, 498, 379
Dressler A., 1980, ApJ, 236, 351
Ellison S. L., Patton D. R., Simard L., McConnachie A. W., Baldry I. K., Mendel J. T., 2010, MNRAS, 407, 1514
Fisher K. B., Davis M., Strauss M. A., Yahil A., Huchra J. P., 1994, MNRAS, 267, 927
Fry J. N., Gaztanaga E., 1993, ApJ, 413, 447
Garilli B. et al., 2008, A&A, 486, 683
Giovanelli R., Haynes M. P., Chincarini G. L., 1986, ApJ, 300, 77
Grützbauch R., Conselice C. J., Varela J., Bundy K., Cooper M. C., Skibba R., Willmer C. N. A., 2010, MNRAS, in press
Guzzo L., Strauss M. A., Fisher K. B., Giovanelli R., Haynes M. P., 1997, ApJ, 489, 37
Guzzo L. et al., 2000, A&A, 355, 1
Hamilton A. J. S., 1988, ApJ, 331, L59
Hawkins E. et al., 2003, MNRAS, 346, 78
Hermit S., Santiago B. X., Lahav O., Strauss M. A., Davis M., Dressler A., Huchra J. P., 1996, MNRAS, 283, 709
Ilbert O. et al., 2009, ApJ, 690, 1236
Iovino A., Giovanelli R., Haynes M., Chincarini G., Guzzo L., 1993, MNRAS, 265, 21
Iovino A. et al., 2010, A&A, 509, A40
Kitzbichler M. G., White S. D. M., 2007, MNRAS, 376, 2
Koekemoer A. M. et al., 2007, ApJS, 172, 196
Kovač K. et al., 2010, ApJ, 718, 86
Landy S. D., Szalay A. S., 1993, ApJ, 412, 64
Le Fèvre O. et al., 2003, in Guhathakurta P., ed., Proc. SPIE Vol. 4834, Discoveries and Research Prospects from 6- to 10-Meter-Class Telescopes II. SPIE, Bellingham, p. 173
Le Fèvre O. et al., 2005, A&A, 439, 877
Leauthaud A. et al., 2007, ApJS, 172, 219
Li C., Kauffmann G., Jing Y. P., White S. D. M., Börner G., Cheng F. Z., 2006, MNRAS, 368, 21
Lilly S. J., Le Fèvre O., Hammer F., Crampton D., 1996, ApJ, 460, L1
Lilly S. J. et al., 2007, ApJS, 172, 70
Lilly S. J. et al., 2009, ApJS, 184, 218
Lintott C. J. et al., 2008, MNRAS, 389, 1179
Lotz J. M., Primack J., Madau P., 2004, AJ, 128, 163
Loveday J., Maddox S. J., Efstathiou G., Peterson B. A., 1995, ApJ, 442, 457
Loveday J., Tresse L., Maddox S., 1999, MNRAS, 310, 281
McCracken H. J., Ilbert O., Mellier Y., Bertin E., Guzzo L., Arnouts S., Le Fèvre O., Zamorani G., 2008, A&A, 479, 321
Madgwick D. S. et al., 2003, MNRAS, 344, 847
Mann R. G., Peacock J. A., Heavens A. F., 1998, MNRAS, 293, 209
Meneux B. et al., 2006, A&A, 452, 387
Meneux B. et al., 2008, A&A, 478, 299
Meneux B. et al., 2009, A&A, 505, 463
Mo H. J., White S. D. M., 1996, MNRAS, 282, 347
Narayanan V. K., Berlind A. A., Weinberg D. H., 2000, ApJ, 528, 1
Norberg P. et al., 2001, MNRAS, 328, 64
Norberg P. et al., 2002, MNRAS, 332, 827
Norberg P., Baugh C. M., Gaztañaga E., Croton D. J., 2009, MNRAS, 396, 19
Park C., Vogeley M. S., Geller M. J., Huchra J. P., 1994, ApJ, 431, 569
Peebles P. J. E., 1980, The Large-Scale Structure of the Universe. Princeton Univ. Press, Princeton, NJ, p. 435
Pollo A. et al., 2005, A&A, 439, 887
Pollo A. et al., 2006, A&A, 451, 409
Porciani C., Giavalisco M., 2002, ApJ, 565, 24
Postman M., Geller M. J., 1984, ApJ, 281, 95
Scherrer R. J., Weinberg D. H., 1998, ApJ, 504, 607
Scoville N. et al., 2007, ApJS, 172, 1
Sheth R. K., Tormen G., 2002, MNRAS, 329, 61
Skibba R. A., Sheth R. K., 2009, MNRAS, 392, 1080
Skibba R., Sheth R. K., Connolly A. J., Scranton R., 2006, MNRAS, 369, 68
Skibba R. A. et al., 2009, MNRAS, 399, 966
Springel V. et al., 2005, Nat, 435, 629
Swanson M. E. C., Tegmark M., Blanton M., Zehavi I., 2008, MNRAS, 385, 1635
Tasca L. A. M. et al., 2009, A&A, 503, 379
Wang L., Li C., Kauffmann G., De Lucia G., 2007, MNRAS, 377, 1419
White S. D. M., Frenk C. S., Davis M., Efstathiou G., 1987, ApJ, 313, 505
White S. D. M., Tully R. B., Davis M., 1988, ApJ, 333, L45
Willmer C. N. A., da Costa L. N., Pellegrini P. S., 1998, AJ, 115, 869
Zehavi I. et al., 2002, ApJ, 571, 172
Zehavi I. et al., 2005, ApJ, 630, 1
Zucca E. et al., 2006, A&A, 455, 879
Zucca E. et al., 2009, A&A, 508, 1217

This paper has been typeset from a TEX/LATEX file prepared by the author.